PERGAMON

Journal of Structural Geology 25 (2003) 633–648

JOURNAL OF STRUCTURAL GEOLOGY

www.elsevier.com/locate/jstrugeo

The growth and propagation of synsedimentary faults

Conrad Childs[a,*], Andrew Nicol[a,b], John J. Walsh[a], Juan Watterson[c]

[a]*Fault Analysis Group, Department of Geology, University College Dublin, Belfield, Dublin 4, Ireland*
[b]*Institute of Geological and Nuclear Sciences Ltd, PO Box 30 368, Lower Hutt, New Zealand*
[c]*Fault Analysis Group, Liverpool University Marine Laboratory, Port Erin, Isle of Man, IM9 6JA UK*

Received 1 April 2000; accepted 1 August 2001

Abstract

Offset of each syn-fault horizon across a synsedimentary (i.e. growth) fault records the throw subsequent to its deposition, allowing successive growth stages of a fault to be determined. This technique has been applied to synsedimentary faults mapped on 3D seismic datasets to distinguish between faults which propagated laterally during growth, faults which did not propagate laterally for significant growth periods and faults in which the lateral dimensions of the active surface decreased during their growth. These different fault tip-line behaviours result in characteristic lateral and dip-parallel fault displacement variations.

Fault propagation rates have been measured for 10 fault tips. The maximum propagation rate is 15 km/My for gravity driven faults and 3 km/My for tectonically driven faults. Rates of fault propagation decrease with elapsed time from the initiation of faulting, with tip-line stasis and retreat becoming dominant in the later stages of fault growth. Static and retreating lateral tip-lines are associated with overlap of the fault strain field with that of a neighbouring fault most often with the formation of a fault relay zone.

Keywords: Synsedimentary fault; Propagation rate; Tip-line; Fault growth

1. Introduction

Sediment thickness changes across a synsedimentary fault (i.e. growth fault) record the differences in elevation of the depositional surface on the footwall and hanging wall sides of the fault through time. These thickness changes, although modified by compaction, allow the fault throws subsequent to the deposition of each horizon, and hence the fault movement history, to be determined. With the increased availability of high quality 3D seismic data, providing several cross-sections across an individual fault, analysis of thickness changes along the whole length of a fault is now feasible. This type of data therefore allows analysis of both the displacement history and the propagation history or growth of individual fault surfaces, methods for which have previously been described by Petersen et al. (1992) and Childs et al. (1993). Numerous descriptions of the distribution of displacement over the surfaces of blind normal faults have been published (e.g. Barnett et al., 1987; Walsh and Watterson, 1987; Nicol et al., 1996), but relatively few concern displacement distributions on surfaces of synsedimentary faults (e.g. Childs et al., 1995; Nicol et al., 1996; Rowan et al., 1998). The movement and propagation histories of several synsedimentary faults, from a variety of tectonic and sedimentary settings, are described here with the aim of establishing and illustrating the main processes which control their displacement distributions. The faults described display a range of behaviours, from those which propagate through time to those for which the active fault trace length decreases. Propagation rates for 10 fault tips have been estimated for all or a part of their growth histories. These data are intended to provide quantitative constraints on fault growth models.

The analysis of fault movement history from across-fault thickness changes is subject to some limitations imposed by the data and by geological relationships. Fault movement and propagation histories have been inferred from the distribution of sediments on the hanging walls of normal faults where the footwalls are emergent (Schlische, 1991; Morley, 1999; Contreras et al., 2000), and from the terraces in uplifted footwalls of active normal faults (Jackson and McKenzie, 1983; Morewood and Roberts, 1999) but neither of these methods is based on accurate measures of the fault throw, i.e. the vertical component of displacement. This is only possible where sedimentation rates exceed fault displacement rates and fault scarps are rapidly blanketed by sediment, such that the fault displacement history is

* Corresponding author. Tel.: +353-1-716-2606; fax: +353-1-716-2607.
E-mail address: fault@fag.ucd.ie (C. Childs).

0191-8141/02/$ - see front matter © 2002 Elsevier Science Ltd. All rights reserved.
PII: S0191-8141(02)00054-8

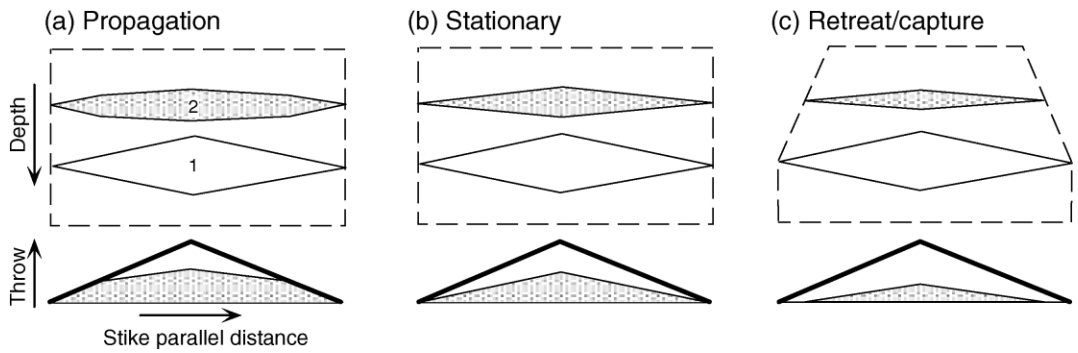

Fig. 1. Diagrammatic representations of the three categories of lateral tip-line development on synsedimentary faults. Unshaded rhombohedra show horizon separations (defined by footwall and hanging wall horizon cutoff lines) for pre-fault horizons (labelled 1) on strike-projections of fault surfaces (broken lines). Stippled areas are separation diagrams for syn-faulting horizons (labelled 2). Horizontal profiles of fault throw are plotted below their respective strike-projections. The bold triangle shows the throw profile for the pre-fault horizon which comprises throws accumulated prior to (unshaded) and since (stippled) deposition of Horizon 2. (a) The lateral extent of the throw accumulated after deposition of Horizon 2 exceeds that before deposition of Horizon 2 indicating lateral tip-line propagation during synsedimentary growth. (b) The lateral extent of throw accumulation before and after deposition of Horizon 2 is the same and a constant throw gradient on the syn-fault horizon results from no lateral tip-line propagation during synsedimentary fault growth. (c) A shorter lateral extent of throw accumulation after deposition of Horizon 2 results from lateral retreat of the tip-line in the synsedimentary growth stage.

preserved as thickness and displacement changes in the syn-faulting sequence. Such faults provide the basis for our study and represent a type of fault often referred to as ‘growth faults’; for the purposes of this article on fault growth we use the more general term ‘synsedimentary fault’ to avoid confusion. Quantification of displacement rates and tip-line propagation rates is also limited by the accuracy with which the ages of mapped horizons can be determined. Rates are time-averaged over intervals determined by the minimum time intervals between mapped and dated horizons. Sediment compaction and unidentified variations in seismic interval velocities are additional sources of uncertainty contributing to inaccuracies in estimates of displacement and propagation, in contrast to the robustness of the qualitative conclusions drawn from them.

Synsedimentary faults can be tectonically or gravity driven and examples of both are described below. With tectonic synsedimentary faults there is usually a clearly defined ‘basement’ to the growth, or syn-fault, interval as is the case for large faults in the North Sea for example, whereas the concept of ‘basement’ is not applicable to gravity-driven synsedimentary faults exemplified by those in the Gulf of Mexico. Nevertheless, the activity of all or part of a fault surface may post-date a particular interval in a syn-faulting sequence, so the terms syn- and post-sedimentary may not only distinguish one fault from another but may also distinguish between parts of the same fault surface active at different times. Similarly, a sedimentary horizon may be pre-fault in one place and syn-fault in another, with respect either to a single fault or to different faults.

The main factors determining the displacement distribution within the syn-faulting sequence on an isolated synsedimentary fault are the rates of sedimentation and of lateral tip-line propagation relative to the displacement rate. If the sedimentation rate is only slightly higher than the displacement rate the hanging wall stratigraphic thickness will be significantly greater than the footwall thickness, growth indices will be high and displacements will decrease rapidly upwards within the growth sequence. Growth index is defined here as (hanging wall thickness − footwall thickness)/footwall thickness. Expressed in this way the growth index is equivalent to the ratio between the relative rates of throw and footwall sedimentation. If the sedimentation rate greatly exceeds the fault displacement rate, growth indices will be low and dip-parallel displacement gradients within the growth sequence will be low, i.e. displacements will decrease slowly upwards. In these circumstances, the growth index and related displacement gradients may be within the range for post-sedimentary faults and would therefore be too low to characterise the fault movement as synsedimentary.

The effects of lateral tip-line propagation on the fault displacement distribution are quite subtle, but nevertheless predictable. These effects are illustrated on the schematic strike-projections and the lateral profiles of throw presented in Fig. 1; a strike-projection plane is the vertical plane parallel to the strike of the fault on which fault displacement variations and horizon cutoffs can be mapped. The three basic types of possible tip-line behaviour are represented by (a) propagating, (b) stationary, and (c) retreating tip-lines, each of which will result in a characteristic fault surface displacement pattern. Where a fault has propagated in the interval between deposition of Horizons 1 and 2 (Fig. 1a) the lateral extent of the throw accumulated after deposition of Horizon 2 exceeds that before deposition of Horizon 2. In this case the throw on Horizons 1 and 2 is the same on the newly formed fault trace length, i.e. close to the fault tips. The previous locations of the lateral tip-points of the fault are the points of divergence of the throw profiles for Horizons 1 and 2 marked by the change in the slope of the throw profile for Horizon 2. Where the tip-points of the fault have remained stationary (Fig. 1b), the throw on Horizon 1 is everywhere greater than that on Horizon 2 and the throw profiles diverge at the present day tip-points. Where the

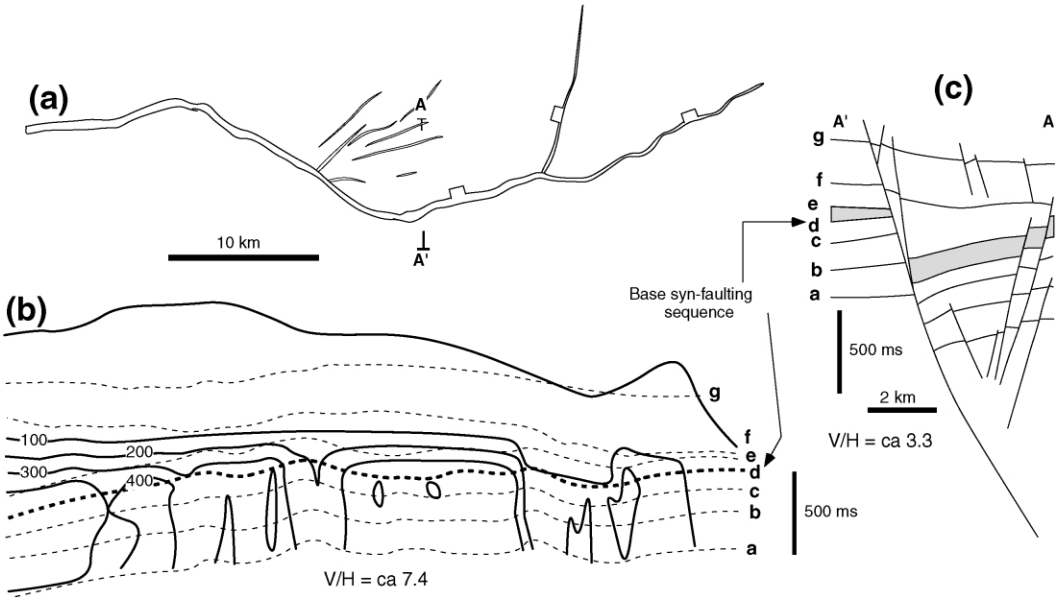

Fig. 2. (a) A large synsedimentary fault from the North Sea as seen on a map of pre-faulting Horizon d. (b) Throw contoured strike-projection of fault, viewed from the footwall side, with contours (solid lines) in ms TWT (1 ms = ca. 1.5 m) and the uppermost contour representing the zero throw upper tip-line. Horizon traces on the fault surface (taken as midway between footwall and hanging wall cutoffs) are shown by broken lines with the base syn-faulting Horizon d shown by the heavy broken line. The strike-projection is aligned with and on the same scale as map (a). (c) Cross-section along line A–A′ on map (a). Note the difference in thickness of the syn-faulting sequence (Horizons d–g) in footwall and hanging wall.

length of the active fault trace has decreased through time (Fig. 1c) the fault trace length is shorter on Horizon 2. The systematics of these simple models can be used as a basis for interpreting displacement patterns on real faults and to derive qualitative descriptions of the tip-line evolution. Each of the model displacement distributions illustrated in Fig. 1 has been recognised in faults mapped from 3D seismic reflection data and the description and analysis of these faults comprise the main body of this article. Determination of tip-line behaviour through time on the basis of throw profiles as described above is equivalent to backstripping fault throws by subtracting the throws on a syn-fault horizon from those of older syn-faulting horizons.

There is often a temptation to over-interpret data obtained from interpretation of seismic images, which have an imprecision not reflected in unambiguous fault diagrams. As the seismic data we have used are of different vintages, and from different depths in different sequences, the resolution varies but an attempt has been made in each case to limit the conclusions to those justified by the data resolution. The throw below which a fault may not be seismically resolvable in the areas examined is between 5 and 10 ms TWT, equivalent to 6–13 m. This resolution limit means that mapped fault tip-lines and tip-points, which are drawn at ‘seismic-zero’ throw, could actually represent the 13-m-throw contour, so faults could extend for significant distances beyond the mapped tip-lines and tip-points. However an accurate estimate of the lateral extent of faults can usually be determined by lateral extrapolation of the observed throw profiles (i.e. throw gradients) beyond the mapped tips.

2. Controls on fault displacement distribution

The surfaces of many synsedimentary faults comprise regions in which a pre-fault sequence is offset and regions in which a syn-fault sequence is offset; a typical synsedimentary fault is illustrated in Fig. 2. The surfaces of other synsedimentary faults may lie entirely within a syn-fault sequence. Displacement distributions on those parts of synsedimentary faults within a pre-fault sequence are subject to the same controls as those on blind faults. Although the hanging wall and footwall deformation associated with blind faults is different from that of synsedimentary faults which intersect the earth’s surface (Savage, 1966; Jackson and McKenzie, 1983; Gibson et al., 1989), the displacement gradients on synsedimentary faults within the pre-faulting sequence are expected to be similar to those of blind faults because these are determined mainly by the physical properties of the faulted sequence (Walsh and Watterson, 1989; Wibberley et al., 1999). The maximum displacement on a synsedimentary fault which intersects a pre-fault sequence is often seen to be at, or close to, the top of that sequence (Nicol et al., 1996), as in Fig. 2b. Where the horizontal dimension of a fault is much larger than the seismically imaged thickness of the pre-faulting sequence, as is usually the case with large faults, the strike-projection will have a high aspect ratio and will show only the uppermost part of a fault surface (Fig. 2). A consequence of these factors is that the displacement contours drawn on the observed parts of the pre-fault sequence will be approximately vertical (Fig. 2b). Within the syn-fault sequence the dip-parallel displacement gradients are high

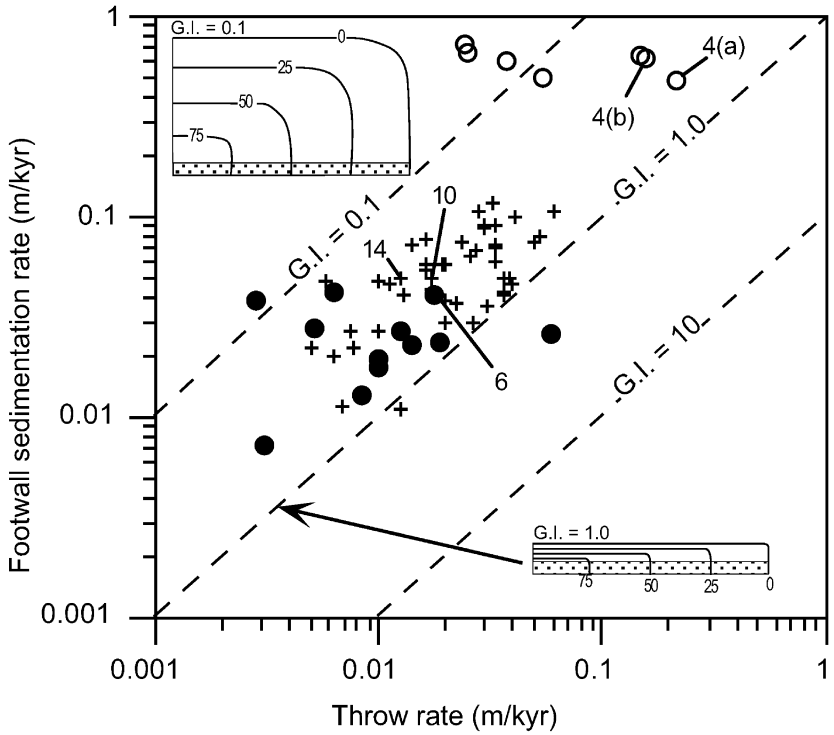

Fig. 3. Maximum throw rate versus sedimentation rate for synsedimentary faults from the Gulf Coast, USA (open circles), the North Sea (crosses) and the Timor Sea (filled circles), with contours of growth index shown (broken lines). Inset diagrams show throw contoured fault surfaces (metres) with pre-fault sequences (shaded) overlain by syn-fault sequences (plain) for growth indices of 0.1 (top left) and 1.0 (bottom right). The maximum throw is 100 m and the vertical dimension of the syn-faulting sequences are 1 km and 100 m for growth indices of 0.1 and 1, respectively. Higher growth indices result in greater differences between the horizontal and vertical spacings of throw contours. The faults described in detail are labelled with the figure numbers of their strike-projections.

relative to the lateral gradients and the displacement contours are approximately horizontal. The boundary between the sub-vertical and the sub-horizontal contours separates the pre- and syn-fault local regions of a fault surface and is generally, with some crucial exceptions, sub-parallel to the lithological layering (Fig. 2b).

2.1. Sedimentation versus displacement rate

Given the proviso of no persistent fault scarp, the relative rates of footwall sedimentation and of fault throw determine the growth index and, therefore, the dip-parallel displacement gradient within the syn-faulting sequence. Fig. 3 is a plot of footwall sedimentation rate versus maximum throw rate for 61 synsedimentary faults from three sedimentary basins, together with contours of equal growth index. With decrease in growth index the vertical separation of the throw contours increases (Fig. 3, insets). Growth indices of <0.1, i.e. footwall sedimentation rates >10 times the throw rates, are associated with dip-parallel throw gradients within the range of gradients occurring on post-sedimentary faults, which are accommodated by volumetric strain of the surrounding rock volume (Walsh and Watterson, 1989) rather than by primary thickness differences. Because of the different rates of footwall uplift on faults of different size, footwall sedimentation rates may vary independently of regional sedimentation rates, but the wide spread of footwall sedimentation rates on North Sea faults (Fig. 3) owes more to the varying rates of regional subsidence and sedimentation over the large area (Inner Moray Firth to North Viking Graben) from which the data are derived. The fewer Timor Sea data (Fig. 3) are derived from a more limited area but still show a significant range of footwall sedimentation rates. The Gulf Coast data are from a limited area with uniformly high footwall sedimentation rates.

2.2. Fault size

Regardless of their size, synsedimentary faults with the same ratio between sedimentation rate and throw rate will have a similar fault surface displacement pattern. Fault size is, therefore, not a primary control on displacement contour patterns. However, within a given area, characterised by a relatively uniform sedimentation rate, faults of different sizes will have markedly different displacement patterns. The three normal faults shown in Fig. 4 each offset a Gulf Coast sequence for which the average footwall sedimentation rate was 0.8 m/ky. These three gravity-induced faults show the range of throw patterns which are common in synsedimentary faulted sequences and the differences between them arise not only from their size differences but also from the different lengths of time for which they were active.

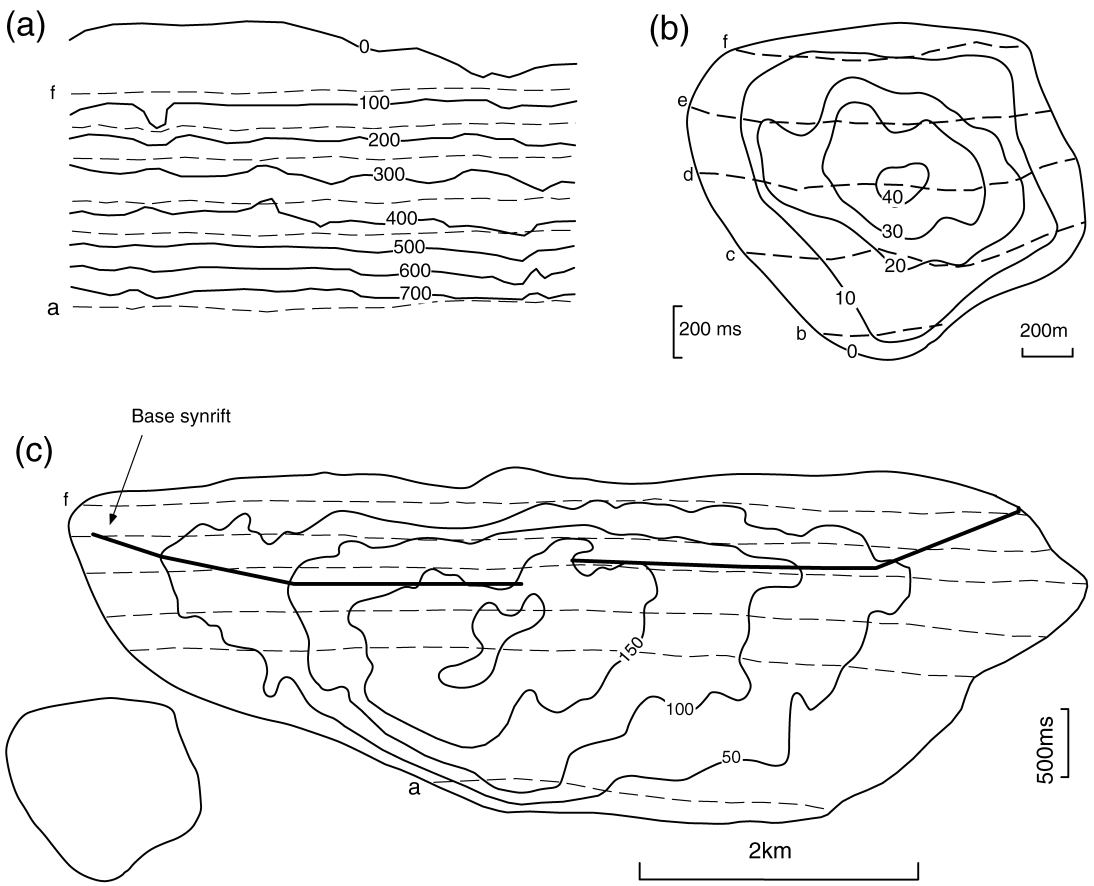

Fig. 4. Varying throw contour patterns (solid lines) on strike-projections of faults of different sizes within the same sequence (Horizons a–f, broken lines), from the Gulf Coast, USA. (a) and (c) are drawn at the same scale and the inset to (c) is an outline of the fault in (b) drawn to scale. Horizon traces are taken as midway between footwall and hanging wall cutoffs. Throw units are ms TWT (1 ms = 1.25 m). (a) A small portion of the uppermost part of a large fault showing sub-horizontal throw contours sub-parallel to horizon traces. The trace length of the entire fault is greater than 10 km. All the horizons shown are syn-faulting with respect to this fault. (b) Small post-sedimentary fault. (c) Medium sized fault showing closer spacing of contours within the syn-fault sequence. The separation line between pre- and syn-fault sequences (bold) cuts across horizon traces (see text) and its position can be inferred from the form of the contours.

The fault shown in Fig. 4a has a maximum observed throw of ca. 0.94 km (750 ms TWT) at the base of the interpreted sequence, from where it decreases uniformly upwards. The lateral extent of the fault exceeds 10 km. Growth indices are >0.55 over the whole of the mapped fault surface and the throw pattern, with approximately horizontal throw contours, is characteristic of large synsedimentary faults. This fault was active throughout the period of deposition of Horizons a to f. By contrast, the fault in Fig. 4b, with a maximum throw of ca. 50 m and growth indices in the range from 0 to 0.08, has a throw contour pattern typical of isolated blind faults (Barnett et al., 1987) with contours symmetrical about the point of maximum displacement in the centre of the fault surface. There is no indication that this fault intersected the free surface at any time during its growth and it is interpreted as having formed as a blind post-sedimentary fault which post-dated Horizon f.

The third fault (Fig. 4c) is intermediate between the previous two and is representative of the majority of synsedimentary faults in that it offsets a pre- and a syn-faulting sequence. The maximum displacement is located near the centre of the fault surface, as on the fault in Fig. 4b, but on the top third of the fault surface throw contours are sub-horizontal. The separation line joining the turning points on individual contours from sub-vertical to sub-horizontal, separates an upper part of the fault surface, with sub-horizontal contours, from the lower part with concentric contours comparable with those in Fig. 4b. Growth indices within the upper part of the fault range from 0.4 in the middle, to 0.01 towards the lateral tip regions. Although some of the growth indices on the uppermost part of the fault are lower than those which are unambiguously diagnostic of synsedimentary movement, the sub-horizontal throw contours and the high growth indices over the central parts of the fault are sufficient to demonstrate coeval sedimentation and fault movement.

The sub-horizontal throw contours on this fault (Fig. 4c) demonstrate that, within the syn-fault sequence, the lateral throw gradients are much lower than the dip-parallel gradients, as is expected on a synsedimentary

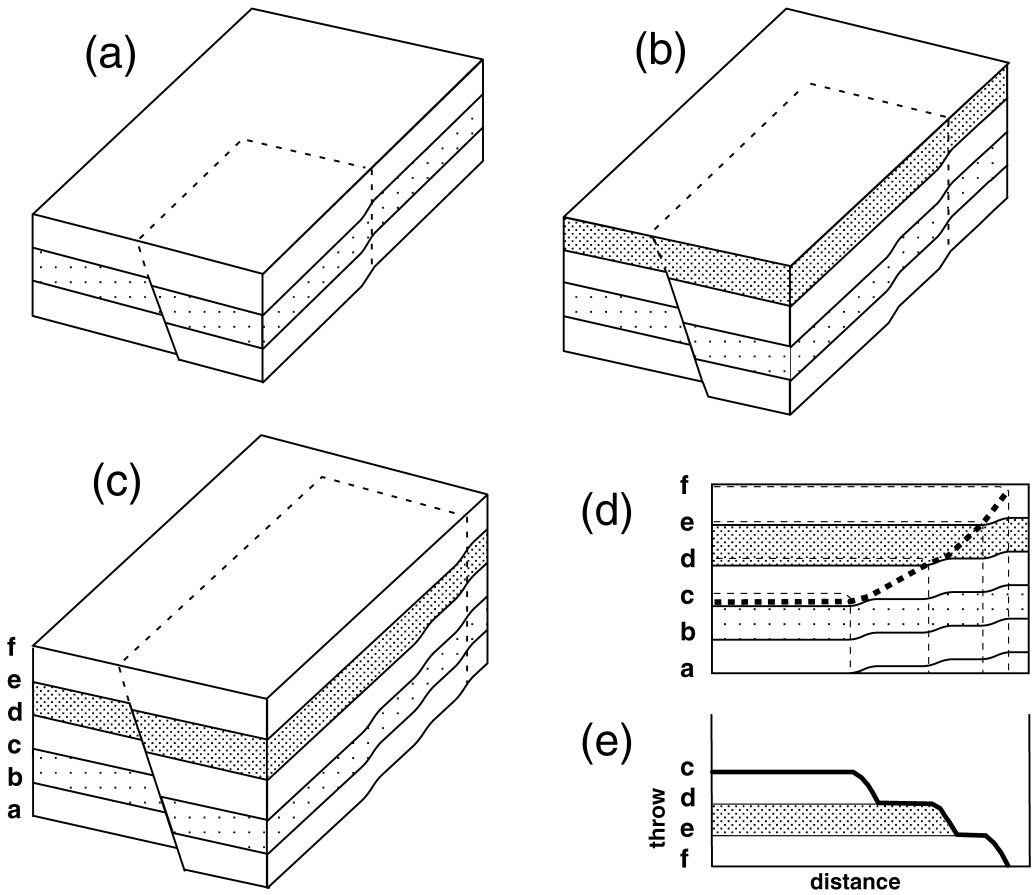

Fig. 5. (a)–(c) Growth stages of part of a synsedimentary fault, showing upward and lateral propagation. Horizon c is the base of the syn-fault sequence, within which the lateral extent of hanging wall thickening increases upwards. (d) Strike-projection with horizon traces of the hanging wall sequence on fault (c) on which all displacement is accommodated by hanging wall subsidence, i.e. horizon traces of the footwall sequence (not shown) are horizontal. The outermost of the throw contours (broken lines) is the fault tip-line. The separation line (heavy broken line) separates the local pre- and syn-faulting parts of an overall syn-faulting sequence. (e) Profile of cumulative synsedimentary throw on Horizon c showing the components due to throw increments in sequence intervals c–d, d–e and e–f.

fault. On any horizon cut by a post-sedimentary fault, the length of a fault trace is a function of the maximum throw (or maximum slip increment, see below) on that horizon (e.g. Ranalli, 1977; Watterson, 1986); the same is true for a pre-fault horizon on a synsedimentary fault. However, a syn-fault horizon records only the cumulative throw subsequent to its deposition, while the fault trace length on that horizon is directly inherited from older horizons. Horizons post-dating fault initiation therefore have fault traces with anomalously high ratios of length to throw and consequently, characteristically low lateral throw gradients. A newly deposited horizon that is offset by only a single slip event, will be characterised by lateral displacement gradients that could be as low as 10^{-5} (i.e. those gradients typical of, for example, single earthquake events). Within a syn-fault sequence therefore, throw contours will be sub-horizontal, even where growth indices are too low to clearly indicate synsedimentary movement. We suggest therefore that synsedimentary fault movement can often be identified on the basis of throw contour shape alone.

2.3. Propagation

A separation line divides the locally pre- and syn-fault parts of the sequence which a fault offsets. In the absence of fault propagation, this separation line occurs at the top of the pre-faulting sequence. Where a fault has propagated, the intersections between this separation line and horizon traces indicate the lateral extent of the fault at the times represented by the successive horizons, because they indicate the position of a lateral tip-point of the fault trace on each horizon at the time when each horizon coincided with the depositional surface (Fig. 5). The locus of a separation line relative to the horizon cutoffs therefore records the lateral propagation of a fault, as shown diagramatically in Fig. 5d.

Fig. 4b provides an example of a fault surface separated into two parts by a line joining contour turning points (minimum radius of curvature; Fig. 4b) representing a local division between a pre-fault sequence (below) and the syn-fault sequence (above). Most of the separation line is at approximately the same elevation as the trace of Horizon d,

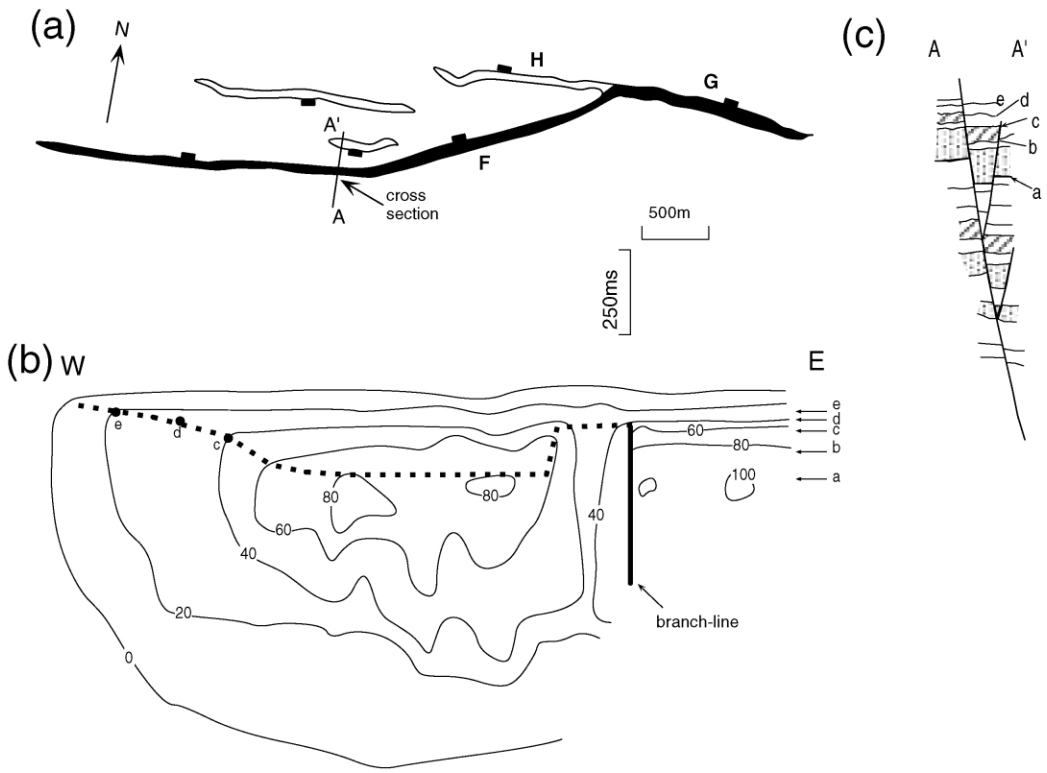

Fig. 6. (a) Map of fault (black fill) on Horizon a from the Timor Sea. A–A′ shows location of cross-section in (c). (b) Throw contoured (ms TWT; 1 ms = 1.2 m) strike-projection of fault in (a), as seen from the footwall side showing separation line between pre- and syn-fault horizons (heavy broken line). Elevations of approximately horizontal horizon traces are shown for Horizons a–e. Abrupt change of elevation of the separation line in the vicinity of the branch-line is due to rapid propagation between deposition of Horizons c and d. The former tip-point on Horizon e was located by extrapolation of the throw profile in Fig. 7. Horizon a is the base of the syn-fault sequence. Position is shown of reclined branch-line with hanging wall splay which became inactive subsequent to deposition of Horizon c. F, G and H are fault segments referred to in text to Figs 7 and 8.

indicating that fault movement began at about the same time as deposition of this horizon. The distal parts of the separation line (Fig. 4b) are curved and oblique to the horizon cutoffs, recording the lateral propagation of the fault.

Further examples of fault lateral propagation interpreted from seismically mapped faults are given below. It is emphasised that propagation, stasis and retreat of lateral tip-lines are not peculiar to synsedimentary faults but their signatures are more obvious if a fault is synsedimentary, because the successive growth stages of the fault are more easily identified and isolated.

3. Examples of fault tip-point kinematics

3.1. Example 1: Propagation of lateral tip-lines

Data for a Tertiary normal fault from the Timor Sea are represented by the map, cross-section and strike-projection in Fig. 6. The fault, F, terminates to the east at a branch-line rather than a free tip-line so only that part of the fault lying to the west of the branch-line complications is considered in detail. On the strike-projection (Fig. 6b), the lower part of the fault surface has the concentric throw contour pattern typical of a pre-fault sequence, whereas the upper part has the predominantly horizontal contours associated with a syn-fault sequence. The separation line joins the turning points of throw contours and intersects traces of successively younger horizons, Horizons c–e, towards the lateral tip region. Elsewhere, the separation line coincides approximately with Horizon a, which is the approximate base of the syn-fault sequence, until the hiatus associated with the branch-line. Growth indices within the syn-faulting section vary between 0.5 at the centre of the fault trace and 0.4 at the western margin of the fault and the average footwall sedimentation rate is 40 m/My. Although the separation line can be identified from the throw contours, it is located more accurately from lateral throw profiles along individual horizons (Fig. 7). Each profile has two distinct segments; one segment includes the maximum throw value and has low lateral throw gradients (approaching zero for the younger horizons) and the other includes the tip region and has relatively high throw gradients (0.035). The point of abrupt change of slope of the throw profiles moves progressively nearer to the tip-point on progressively younger horizons. On the central parts of the profiles, the near constant throw along each horizon increases with the age of the horizon, whereas on the more distal parts of the profiles the throws on all horizons are similar.

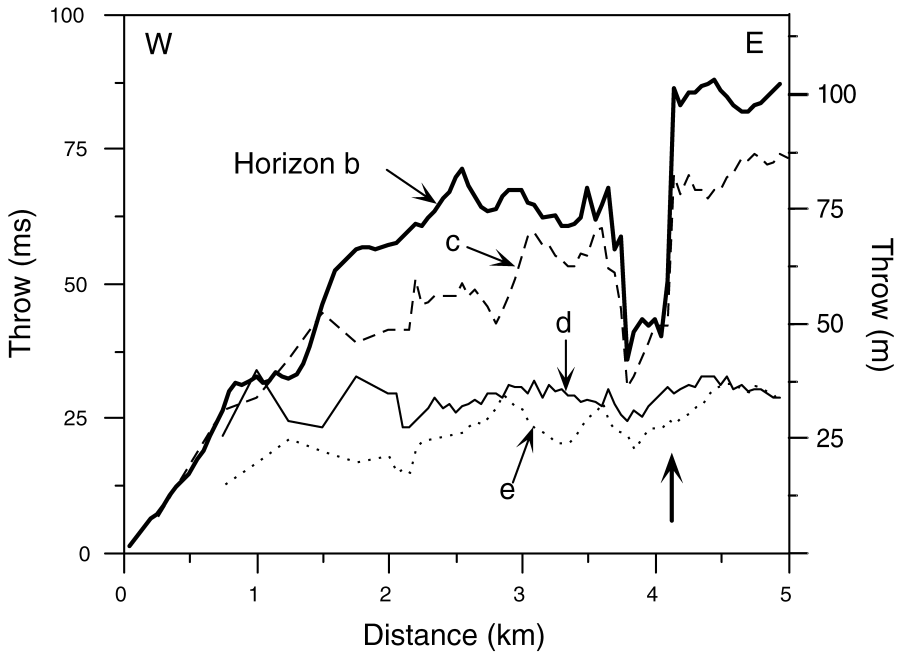

Fig. 7. Throw profiles along syn-fault horizons (b–e) intersected by the fault shown in Fig. 6. The hiatus in profiles along Horizons b and c (arrowed) marks the branch-line which post dates these horizons. Prior to formation of the branch-line segment F (Fig. 6) was a separate fault and segments G and H comprised a single fault (see Childs et al., 1995). Accuracy of throw values is ±6 ms (5 ms TWT).

As the separation line defines the lateral tip-point of the fault at the time of deposition of each horizon, the rate of lateral tip-line propagation can be determined. The lateral tip-line of this fault propagated ca. 1.6 km laterally between deposition of Horizons c and the end of fault movement, during which time the maximum throw increased by ca. 70 m, approximately trebling its previous value. Direct age data are not available for horizons b–e in the Timor Sea fault shown in Fig. 6. The only age estimate available is for the base of the synfaulting sequence (Horizon a), which coincides with the Base Pliocene (5.3 Ma; Woods, 1992). Assuming an approximately constant sedimentation rate to the present day (which is supported by constraints from adjacent areas within the Timor Sea), the upper tip-line, ca. 50 m below the present day sea-level, indicates that fault movement ceased ca. 0.8 Ma. The maximum throw on this fault of ca. 100 m accrued over a 4.7 My period. In the ca. 2.35 My period between deposition of Horizon c and the end of activity of this fault it increased in length by 1.6 km at an average propagation rate of 0.7 km/My (Fig. 8). The estimated propagation rates for the individual mapped intervals and the associated errors are given in Table 1 and described in Section 4.

The determination of propagation rates relies on establishing both the present day and former locations of the lateral fault tip-line. In this example, the present day tip-line location is well constrained by extrapolation of the throw profile for Horizons b and c to the west and the associated errors are negligible. The error associated with estimation of the lateral position of former tip-line locations, which relies on determining the points of intersection between the throw profiles for two horizons and/or the inflection points on individual throw profiles, is likely to be more significant. The error in measurement of individual throw readings for this dataset is ca. ±6 m, however the error associated with determining best fit lines through several throw values on a throw profile is significantly less. We estimate that a best fit line can be drawn through a straight portion of a throw profile to an accuracy of ±2–3 m. When determining the point of intersection between two straight line portions of a profile, for example on Horizon c, the error in estimate of its along strike location is, for this dataset, at most ca. ±200 m. The error associated with the interval between deposition of Horizon c and the end of fault activity is estimated to be ±0.5 Ma and the propagation rate lies within the range 0.49 to 0.97 km/My, a level of accuracy which is acceptable for the purposes of this article.

The difference in throw between Horizon b and a younger horizon in Fig. 7 shows the distribution of cumulative throw along the fault trace at the time of deposition of the younger horizon. Inspection of the differences in throw between Horizon b and each of c, d and e demonstrates that the point of maximum cumulative throw on the fault trace has remained more or less static during lateral propagation of the western tip of the fault.

Thus far only the propagation of the western tip region of the fault has been considered. As described by Childs et al. (1995), to the east fault segment F links with a larger fault, comprising segments G and H. Linkage occurs along a branch-line, seen as a branch-point on the map (Fig. 6a), at about the time of deposition of Horizon d. Throw contours above Horizon d (Fig. 6b) are horizontal and continuous

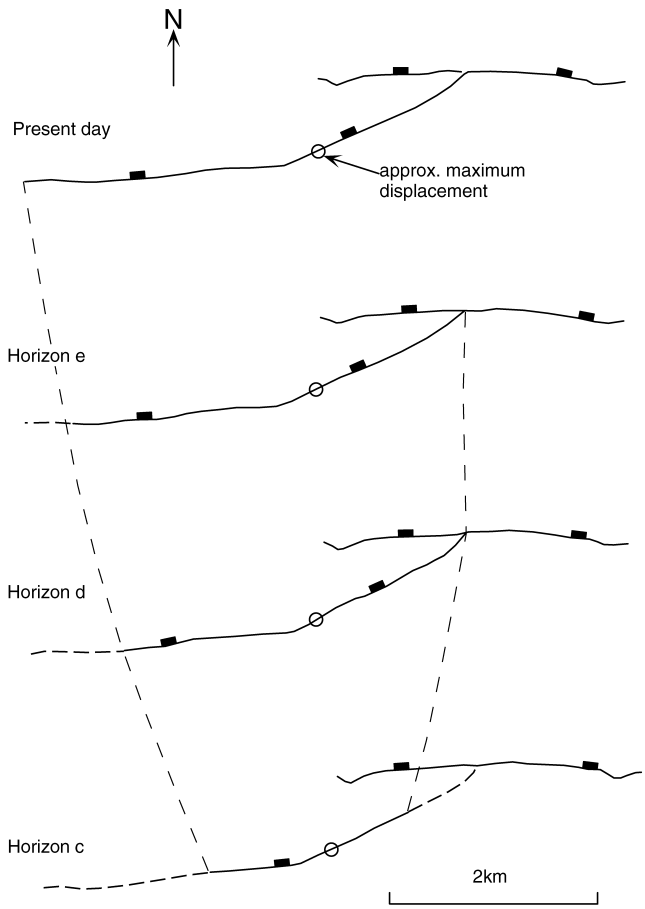

Fig. 8. Interpreted growth stages of the fault in Fig. 6 shown as fault traces on each horizon at the time each horizon was at the surface (solid lines), showing segment F (see Fig. 6) as a separate fault with two free tip-points, and segments G and H comprising a single fault at the time of Horizon c. Subsequent development of the tip-points of segment F is shown by steep broken lines. The western (left) tip-point propagated laterally and remains a free tip-point. The eastern tip-point propagated until it intersected the fault comprising segments G and H and became a branch-point, isolating segment H which became inactive. Open circles show points of maximum total throw at each stage.

whereas below this horizon they are discontinuous, a feature which is consistent with fault linkage between the times of deposition of Horizons c and d (Fig. 8). The timing of the formation of this branch-line is tightly constrained by the time at which segment H became an inactive hanging wall splay (Childs et al., 1995). The throw distribution adjacent to the branch-line indicates that between the time of deposition of Horizons c and d, the tip-line propagated laterally ca. 700 m eastwards. For the age resolution of the dataset the propagation of this tip is instantaneous. If a constant sedimentation rate is assumed over the period of fault activity, the period between deposition of horizons c and d is 0.65 My and a minimum propagation rate for this portion of the fault is ca. 1.1 km/My.

3.2. Example 2: Stationary lateral tip-lines

Increase in displacement on an isolated fault is accompanied by a complementary increase in the fault dimensions by radial tip-line propagation (Watterson, 1986). Where faults are not isolated but have overlapping strain fields, the strain fields interact and modify the displacement patterns on both faults. Lateral displacement gradients on the overlapping map traces of subparallel normal faults are steeper than elsewhere on the faults (Walsh and Watterson, 1990) and are accommodated by high strains and bed rotation within the overlap, or relay, zone (Larsen, 1988; Peacock, 1990). In terms of tip-line propagation the high lateral displacement gradients are a consequence of reduction in lateral tip-line propagation rate relative to the displacement rate which, in the limiting case, results in a static tip-line. The relay zone systematics previously established by examination of blind faults (Peacock and Sanderson, 1994; Huggins et al., 1995) are amplified below by reference to a relay zone bounded by synsedimentary faults.

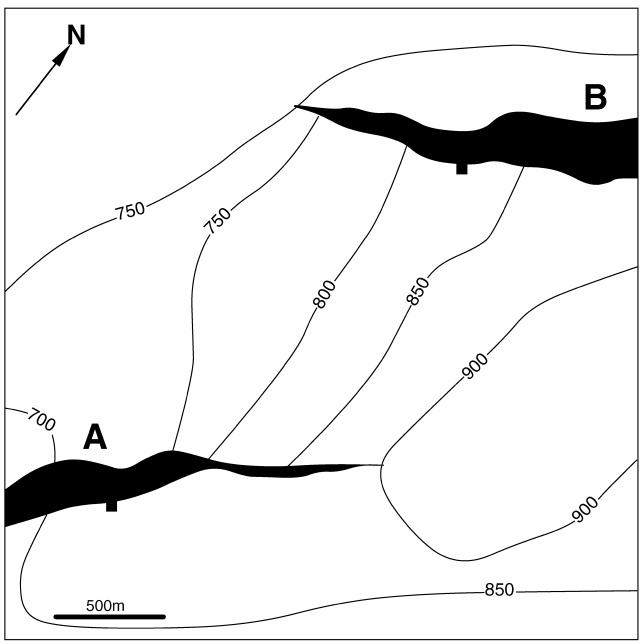

Fig. 9. Overlapping tip regions of fault segments (A and B) bounding a relay ramp, as seen on map of a pre-fault horizon (Horizon a; Figs. 10 and 11), Moray Firth, U.K.C.S. Structure contours are in ms TWT (1 ms = 1.25 m).

A map of a syn-fault horizon in the Moray Firth, U.K.C.S., shows the tip regions of two faults, A and B, which bound a relay zone (Fig. 9); these faults offset both syn-fault and pre-fault horizons. As in previous examples, throw contours on the faults are sub-horizontal within the syn-fault sequence and sub-vertical in the pre-fault sequence, as shown in Fig. 10 for Fault A. Throw profiles along four horizons are shown in Fig. 11 and profiles on the two pre-fault horizons (a and b) show that lateral throw gradients increase from 0.063 (i.e. 0.05 ms/m on Fig. 11) outside the zone of fault interaction to 0.150 (i.e. 0.12 ms/m on Fig. 11) within the relay ramp. The tip region coincides with the lateral extent of bed rotation within the footwall of the fault, consistent with the high lateral displacement

Table 1
Data used in estimation of fault tip-line propagation rates. Of the faults numbered 1 to 10, the first five are presented in detail in the relevant figures. Horizon labels are those used in the figures. Half lengths of faults are measured from the point of maximum displacement on the mapped fault trace to the fault tip-point. The point of maximum displacement of fault 4 lies outside the available data area and the half length given is the entire mapable fault length. Throws for the North Sea, Gulf Coast and Timor Sea data have been depth converted using average seismic velocities of 2.50, 2.50 and 2.40 km/s, respectively. Propagation rates, calculated as the difference in half length divided by the time interval between mapped horizons are positive for increase in fault length and negative for decrease in fault length, i.e. tip-point retreat. Maximum throw values quoted are maximum throws at the base of the syn-faulting sequence backstripped to the time of deposition of each horizon. Fault 4 attained its maximum length and the tip-line retreated prior to deposition of the oldest mapped syn-faulting horizon and the time at which fault propagation stopped is unconstrained. The propagation rate for this point is calculated from the elapsed time to the first mapped syn-faulting horizon and is therefore likely to be a significant underestimate of the actual propagation rate. For fault 5 the initial propagation phase was too fast to be recorded as seismically resolvable thickness variations, again the propagation rate is calculated from the elapsed time to the first mapped syn-faulting horizon

Fault	Horizon	Max throw (m)	Half length (m)		Elapsed time (My)		Time interval (My)		Prop rate (m/My)	Max.	Min.
1. Timor Sea: Fig. 6, W tip	c	31	1210	(±200)	2.35	(±0.5)	2.35	(±0.50)	515	762	354
	d	60	1880	(±200)	3.00	(±0.5)	0.65	(±0.14)	1031	2091	343
	e	69	2410	(±200)	3.40	(±0.5)	0.40	(±0.09)	1325	2953	268
	tip	99	2830	(±200)	4.70	(±0.5)	1.30	(±0.28)	323	801	13
2. Timor Sea: Fig. 6, E tip	c	31	830	(±200)	2.35	(±0.5)	2.35	(±0.50)	353	557	221
	d	60	1580	(±200)	3.00	(±0.5)	0.65	(±0.14)	1154	2247	444
3. Moray Firth: Fig. 9	c	140	9000	(+200)	5.00		5.00	(2.50–10.00)	1800	3680	900
	d	170	9000	(+200)	6.00		1.00	(0.50–2.00)	0	400	−400
	tip	210	9000	(+200)	8.00		2.00	(1.00–4.00)	0	200	−200
4. Moray Firth: Fig. 12	a	0	3900	(+50)	0.00		0.00	(—)	650	—	—
	b	120	3400	(+250)	6.00		6.00	(3.0–12.0)	−83	−250	−21
	c	160	2500	(+250)	8.00		2.00	(1.00–4.00)	−450	−1150	−163
5. Gulf Coast: Fig. 4b, rhs	d	131	2350	(±200)	0.00	(—)	0.00	(—)	2350	—	—
	f	200	3410	(±200)	1.00	(±0.2)	1.00	(±0.20)	1060	1950	550
6. Gulf Coast	—	88	6000	(±200)	0.40	(±0.2)	0.40	(±0.1)	15000	20667	11600
7. Timor Sea	—	25	1597	(±200)	1.30	(±0.5)	1.30	(±0.17)	1228	1595	948
	—	66	1597	(±200)	3.30	(±0.5)	2.00	(±0.27)	0	231	−231
	—	96	1558	(±200)	4.20	(±0.3)	0.90	(±0.12)	−43	463	−563
	—	104	1519	(±200)	4.70	(±0.3)	0.50	(±0.07)	−78	833	−1013
	—	124	1363	(±200)	6.00	(±0.3)	1.30	(±0.17)	−120	217	−493
8. Timor Sea	—	25	880	(±200)	1.30	(±0.5)	1.30	(±0.17)	677	959	462
	—	58	1130	(±200)	3.30	(±0.5)	2.00	(±0.27)	125	375	−87
	—	88	1340	(±200)	4.20	(±0.3)	0.90	(±0.12)	233	782	−244
	—	97	1460	(±200)	4.70	(±0.3)	0.50	(±0.07)	241	1201	−646
	—	117	1460	(±200)	6.00	(±0.3)	1.30	(±0.17)	0	355	−355
9. Timor Sea	—	44	3013	(±200)	1.30	(±0.5)	1.30	(±0.17)	2318	2852	1909
	—	103	3900	(±200)	3.30	(±0.5)	2.00	(±0.27)	444	1245	311
	—	146	3900	(±200)	4.20	(±0.3)	0.90	(±0.12)	0	513	−392
	—	162	3242	(±200)	4.70	(±0.3)	0.50	(±0.07)	−1316	−595	−2442
	—	196	3242	(±200)	6.00	(±0.3)	1.30	(±0.17)	0	355	−355
10. Timor Sea	—	39	3821	(±200)	1.30	(±0.5)	1.30	(±0.17)	2939	3569	2458
	—	124	3821	(±200)	3.30	(±0.5)	2.00	(±0.27)	0	387	−387
	—	160	3821	(±200)	4.20	(±0.3)	0.90	(±0.12)	0	513	−513
	—	178	3821	(±200)	4.70	(±0.3)	0.50	(±0.07)	0	923	−923
	—	210	3821	(±200)	6.00	(±0.3)	1.30	(±0.17)	0	355	−355

gradients on pre-fault horizons being accommodated by strain within the relay ramp. Throw profiles (Fig. 11) along the two syn-fault horizons (c and d) show throws on these horizons to be substantially less than on the pre-fault horizons not only along the main part of the fault trace but also in much of the tip-region. This difference indicates that the lateral extent of the fault was much the same during deposition of the syn-fault sequence as it had been previously, because more throw accumulated on pre-fault horizons in the tip region than on syn-fault horizons (see Fig. 1b). On the distal ca. 250 m of the profiles (Fig. 11) the throws on all four horizons are similar, from which it could be concluded that there was a corresponding amount of synsedimentary lateral propagation, but this would be to over-interpret the imprecise data. It is safe to conclude, however, that there was little or no lateral propagation of the tip-line during the ca. 3 My of syn-fault sedimentation following the deposition of Horizon c, during which time an additional ca. 75 m fault throw was accumulated.

In the 5 My period between deposition of the youngest mapped pre-fault horizon (Horizon b) and Horizon c the fault attained a half length of ca. 9 km, giving an average propagation rate of 1.8 km/My. Although the mapped horizon throws cannot be used to determine the details of

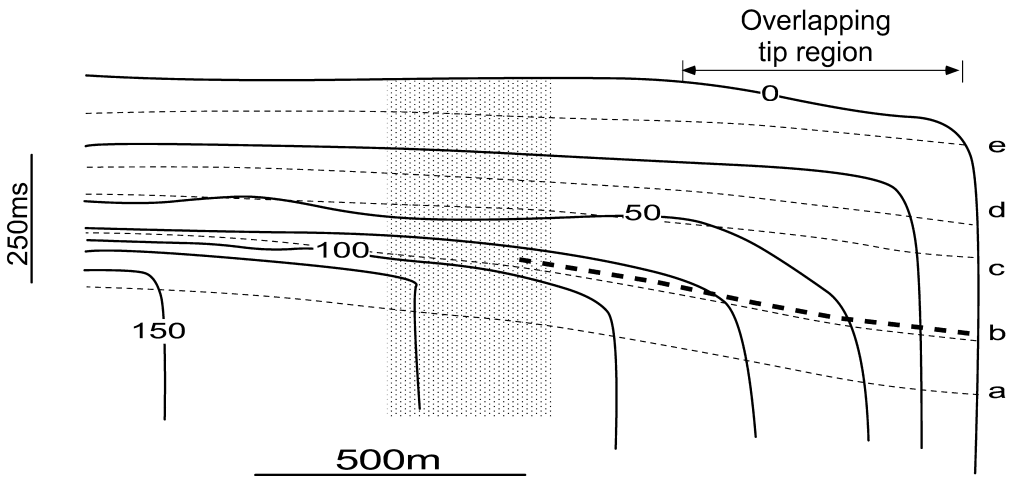

Fig. 10. Strike-projection of Fault A of Fig. 9 with throw contours (ms TWT; 1 ms = 1.25 m) and traces of horizon footwall cutoffs, as viewed from the hanging wall side of the fault. Horizons a and b are pre-fault and Horizons c–e are syn-fault. The bold dashed line is the base of the syn-fault sequence and the stippled area is the approximate location of the edge of the relay ramp. The length of overlap of the relay bounding faults (ca. 500 m) is not equal to the length of the relay ramp.

the tip-line behaviour in the c–d interval, interval thickness variations in the footwall of the fault (Fig. 10) suggest that the fault tip-point was at its present location well before deposition of Horizon c. The footwall horizon traces on the strike-projection (Fig. 10) show lateral thickening of the syn-fault intervals (b–c and d–e), due to ramp rotation, extending in both cases all the way to the lateral tip-line. The presence of significant ramp related thickness changes in the b–c interval suggests that ramp rotation was occurring for a large part of this interval during which time the fault tip-line must have been close to its present location. The initial 5 My of fault activity is therefore likely to have comprised an initial period of propagation, which was faster than the 1.8 km/My average value, followed by a period of tip-line stasis.

3.3. Example 3: Retreating tip-line

The active portion of the trace length of a fault can decrease through time. Either an abrupt or a gradual reduction in the active lateral extent of a synsedimentary fault should be marked by a decrease in the length of fault traces, and syn-faulting displacements, on successively younger growth horizons (Fig. 1c). Although not observed on isolated faults, reduced fault trace lengths on younger syn-faulting horizons are common in association with fault linkage and capture, as in the example shown in Figs 12–14.

Fig. 12 shows two faults (F1 and F2) from the Inner Moray Firth, between which there is transfer of displacement so that a southward displacement decrease on F1 is matched by an increase in displacement on F2. The zone of displacement transfer between the two faults is not a simple relay zone as F2 continues for 3 km northward beyond the zone of displacement transfer. Seismic sections across fault F1 show clear evidence of retreat of the fault through time. On seismic line B–B′ (Fig. 13) the fault offsets Horizon c and extends upwards a further 250 m; however, on A–A′ the upper tip-point of the fault is below Horizon c and at this position became inactive before deposition of Horizon c. The strike-projection of F1 (Fig. 14a) shows that the upper tip-line of the southern 1.5 km of the fault plunges to the SW indicating a progressive retreat of the active fault trace. The point of intersection between the tip-line and each horizon is an indication of the active length of the fault trace at the time of deposition of that horizon and the lateral extent of the fault on Horizons a–c is shown on the map of Horizon a (Fig. 12). The throw profiles for successively younger horizons (Fig. 14b) resemble those in Fig. 1c.

Evidence of tip-line retreat relies on establishing the location of the tip-line intersection with each horizon. The location of the tip-line is most accurately determined by extrapolation of throw gradients seen on lateral throw profiles in the tip region to zero throw. For Horizon a the tip-point is at most 50 m beyond the mapped tip and for Horizons b and c the tip-point may be up to 250 m beyond the mapped tip. Even given these uncertainties in the precise tip-line location it is nevertheless clear that the tip-line plunges to the SW. High fault growth indices, particularly in the interval between Horizon a and the upper tip-line (G.I. > 0.3), demonstrate that the upper tip-line elevation is controlled by interaction with the contemporary free-surface and related syn-faulting sequence growth, rather than by post-sedimentary dip-parallel throw gradients. A discontinuity in the upper tip-line occurs at the line of intersection between F1 and a fault connecting F1 and F2. The broken line in Fig. 12 shows the approximate position of the linking fault which offsets only horizons younger than Horizon c. The branch-line with the connecting fault coincides with an increase in the displacement on Horizons b and c. A step in the throw profile for Horizon a (Fig. 14b) is not seen partly because the throw variation on this part of the fault is masked by significant hanging wall normal drag (Fig. 13)

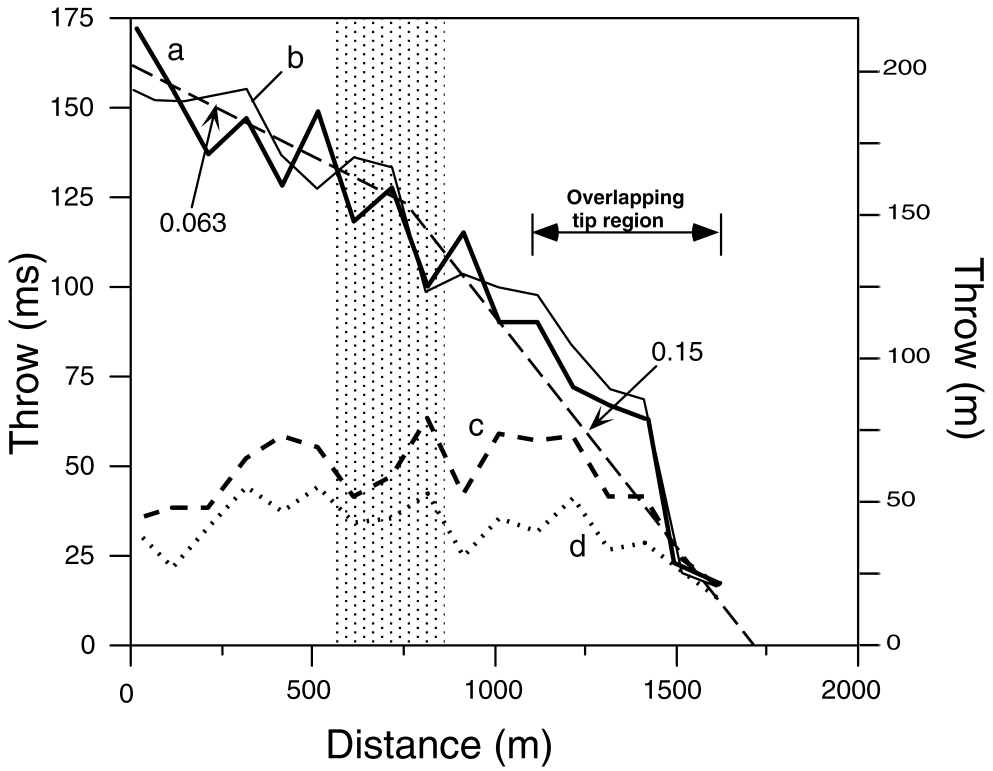

Fig. 11. Throw profiles along the relay bounding segment of Fault A (Fig. 10). Throws on pre-fault Horizons a and b are higher than those on syn-fault Horizons c and d even at the extremity of the fault showing that there was little or no lateral propagation of the fault during deposition of the syn-fault horizons. The stippled area indicates the approximate location of the edge of the relay ramp.

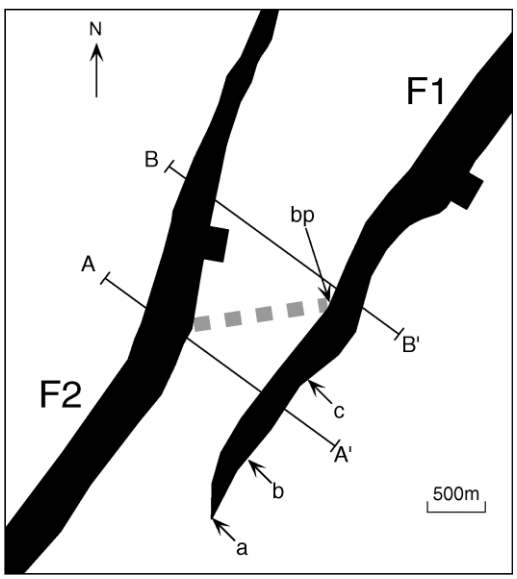

Fig. 12. Map (on Horizon a; Figs. 13 and 14) of overlapping faults bounding a relay zone. The successive locations of the tip-line of F1 at the time of deposition of Horizons a–c are indicated. The approximate location of a relay breaching fault, which offsets only Horizons b and c, is indicated by the heavy broken line. The branchpoint between F1 and the breaching fault is shown (bp). Locations of cross-sections A–A′ and B–B′ (Fig. 13) are indicated.

but mainly because the connecting fault is not seen on deeper levels.

The observed displacement distribution on Fault F1 is interpreted to reflect tip-line retreat due to a progressive narrowing of the zone of displacement transfer between fault F1 and F2, which culminated in the formation of a through-going connecting fault and an inactive hanging wall splay.

3.4. Summary of observations

The complete range of possible tip-line behaviours has been observed. The general conclusion is that fault trace lengths active over geologically significant periods are a function of the tendency for the dimensions of a fault to increase as the displacement increases, unless inhibited by linkage or other interaction with a neighbouring fault, which causes the active dimensions to increase more slowly, remain constant or even to decrease.

4. Propagation rates

Fault tip-line propagation rates have been estimated for all of the faults illustrated. The methods used to define propagation rates have also been applied to other fault tip-lines from Tertiary faults in the Timor Sea and the Gulf Coast. Data on fault propagation rates are listed in Table 1.

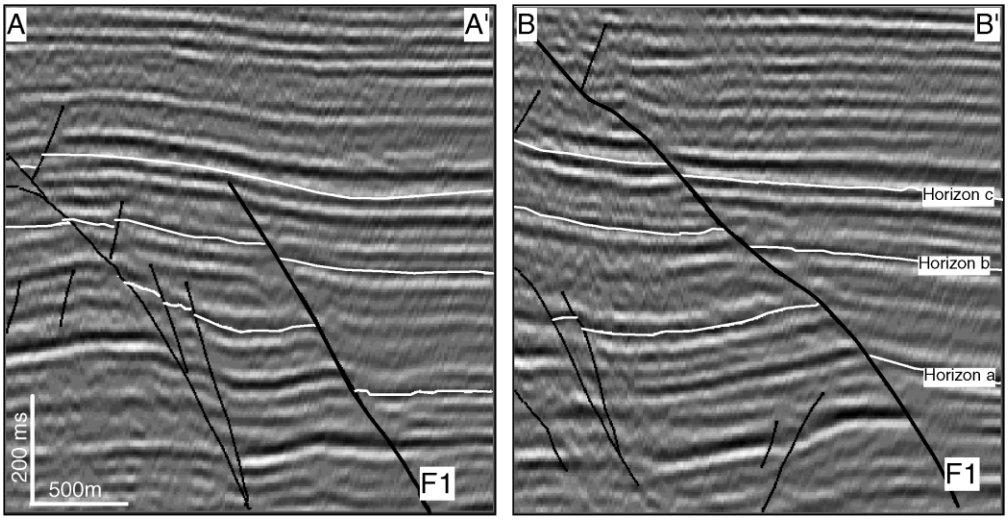

Fig. 13. Interpreted seismic sections across the faults shown in Figs. 12 and 14. Section A–A′ (left) is across the distal part of fault F1. The fault became inactive at this location prior to deposition of Horizon c, as indicated by the upward termination of the fault trace at a tip-point between Horizons b and c. The section across the more proximal part of fault F1 (B–B′) shows the fault trace offsetting Horizon c and shallower seismic reflections.

These data are also plotted on graphs of fault trace half-length versus elapsed time since fault initiation (Fig. 15a) and of propagation rate versus elapsed time since fault initiation (Fig. 15b).

Errors associated with calculation of fault propagation rates derive from uncertainty in estimation of both the present and former tip-line locations and the time intervals over which propagation rates are calculated (Table 1). The method of estimating errors associated with tip-line locations has been described previously for Fig. 6 (Section 3.1). The same approach has been adopted for the additional Timor Sea and Gulf Coast examples. For the Moray Firth examples, which show a static tip-line (Section 3.2) and tip-line retreat (Section 3.3), errors in tip-line location are due only to sub-resolution continuation of the present day mapped fault rather than to the determination of former tip-line locations. Fault lengths for these examples are therefore minimum estimates.

The errors associated with the elapsed times since fault initiation for each mapped horizon are presented in Table 1. Clearly these errors are not applicable to estimation of errors in the time interval between successive horizons. To estimate the time interval errors for the Timor Sea examples we have calculated the error in time interval for the entire faulted sequence and assigned a proportion of this error to each mapped time increment according to its duration. For the Gulf Coast faults, which are less than 5 My old, the error in time interval determination is estimated to be at most ±0.2 My. For the Inner Moray Firth faults which offset an Upper Jurassic sequence the seismically mapped horizons are dated using ammonites from wells within the study area. In the Upper Jurassic the errors in absolute age determinations are ± ca. 3 My, but these errors are not applicable to estimation of errors associated with mapped time intervals. Within the past 20 years published estimates of the duration of the Kimmeridgian and Tithonian Upper Jurassic stages have varied by as much as a factor of three (Gradstein et al., 1995). We have assumed that this variability provides an indication of the likely magnitude of errors associated with the duration of time intervals between mapped horizons in the Inner Moray Firth. We have assigned errors which give a factor of four variation in mapped interval durations where the time interval range is a factor of 0.5–2 times the estimated value.

The most striking feature of Fig. 15a is the paucity of faults which show a simple relationship between elapsed time and fault length. Only faults 1, 2 and 5 (Fig. 15) show a clear positive correlation between time and length. The majority of faults have their highest rate of increase in length in the first time step, (between time zero and the first age at which length is measured) and this is true of Faults 7–10 from the Timor Sea. Many of the Tertiary faults in the Timor Sea area are reactivated faults which initially formed in the Late Jurassic to Early Cretaceous (Woods, 1992; Nicol et al., 1997; Meyer et al., 2002). It is likely that the rapid increase in fault length at the early stages of Tertiary faulting is because the faults have inherited their lengths from pre-existing faults at depth. Fault 1, also from the Timor Sea, which does not link to a large structure at depth (Fig. 6) and is therefore not a reactivated fault, contrasts with Faults 7–10 in that it shows progressive propagation of one free tip throughout its growth history. Three of the fault tips, Faults 4, 7 and 9, retreat through time following an initial propagation phase. The trend for both individual faults and the whole dataset is for propagation rate to decrease with elapsed time (Fig. 15b).

The fault propagation rates derived from synsedimentary faults are time averaged over geologically significant periods (0.4–5 My). The highest measured propagation

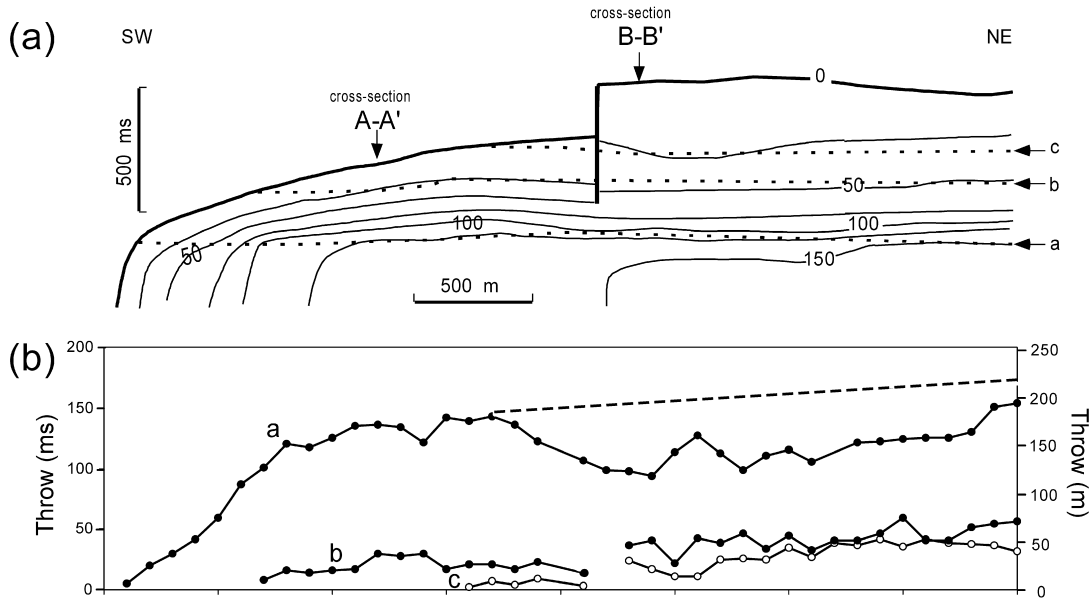

Fig. 14. (a) Throw contoured strike-projection of fault F1 (Fig. 12). The discontinuity in the upper tip-line occurs at the line of intersection with a fault in the footwall. Contour units are ms TWT (1 ms = ca. 1.25 m). Locations of cross-sections A–A′ and B–B′ (Fig. 13) are indicated. (b) Throw profiles for Horizons a–c. The dashed line indicates the magnitude of throw on Horizon a if normal drag is included.

rate is from a Gulf Coast dataset in which 6 km of fault trace length formed in 0.4 My, or 15 km/My. Gulf Coast faults are gravity driven and their rates of propagation may not be comparable with tectonic faults. The highest estimated propagation rate for tectonic faults is ca. 3 km/My.

There are few published data on the rates of propagation of faults. Published rates are derived from geomorphological studies on present day fault scarps. These data are applicable to faults over time scales of 100 s to 100,000 s years but not to the time ranges considered in this article (0.4–5 My). Morewood and Roberts (1999) have determined a lateral propagation rate of 12–16.7 km/My for the surface trace of the South Alkyonides Fault Segment, but suggest that the fault trace at depth has maintained a constant length over a 330 ky period. Jackson and Leeder (1994) have estimated a propagation rate of 50 m per earthquake for a normal fault at Pleasant Valley (USA). Jackson et al. (1996) suggest lateral propagation for thrust related folds of 10–50 m per earthquake for Central Otago (New Zealand), Medwedeff (1992) estimates 25 km/My for propagation of the Wheeler Ridge and Benedetti et al. (2000) a rate of 10–20 km/My for a thrust related growth fold, Montello, Northern Italy. These rates are significantly higher than we have determined. There are many possible explanations for this difference, the most significant of which is likely to be the difference in time over which the propagation rates are measured.

5. Discussion

As with blind faults, most of the complexities seen in synsedimentary faults are due to fault interaction, linkage and capture, usually associated with a relay zone. The effects of relay zones and relay breaching on the connectivity and seal potential of blind faults are amplified in the case of synsedimentary faults by sequence thickness variations within relays and by the potential for sediment transport from footwall to hanging wall along relay zones. The greatest effects on sedimentation are associated with relays on synsedimentary faults with persistent fault scarps (e.g. Gawthorpe et al., 1994; Dawers and Underhill, 2000), which have not been considered in this paper.

The definition of the geometry of growth stages of synsedimentary faults is limited only by the quality of the seismic data and the effort expended in mapping multiple horizons. However, closer definition of the kinematics of fault growth requires a knowledge of the absolute time intervals between mapped horizons and 1 my approaches the best resolution likely to be obtained in a seismically mapped sedimentary sequence (Nicol et al., 1997).

Changes in fault lengths through time in this study were estimated from former tip-line locations represented by the boundary between pre-fault and syn-fault sequences. This boundary is derived from (i) inflection points in contours of throw on fault surfaces, (ii) divergence of throw profiles for horizons deposited at different times, or (iii) changes in throw profile slope. Tip-line locations determined in this way are equivalent to those defined by displacement backstripping of faults, in which the throws on syn-faulting horizons are subtracted from those of older horizons. An alternative backstripping method where the maximum throw on a syn-faulting horizon is subtracted from underlying horizons with the implicit assumption that throw contours represent former tip-lines (e.g. Rowan et al., 1998), is broadly equivalent to the method employed here when applied to faults which have

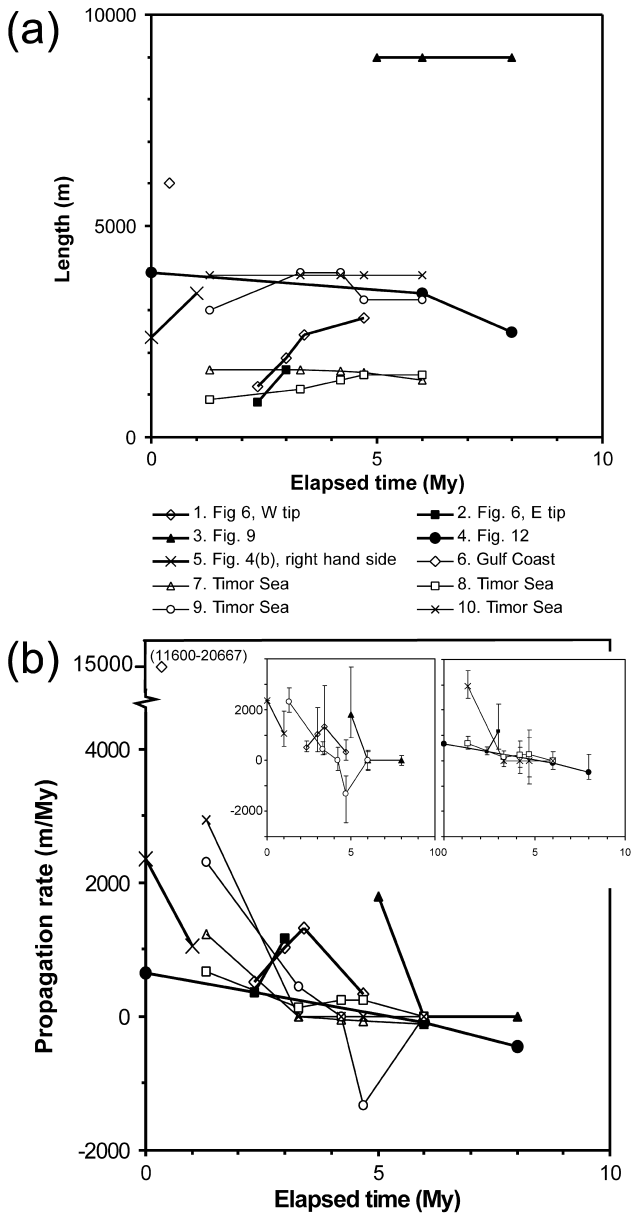

Fig. 15. (a) Curves of fault trace length versus elapsed time since fault initiation for fault tip-lines numbered 1 to 10 (see also Table 1). The heavy lines are for tip-lines discussed in the text. (b) Curves of fault propagation rate versus elapsed time. Inset graphs show the error bars attached to the propagation rate estimates (see Table 1). Error bars for fault 7 are not shown. The key applies to both (a) and (b).

propagated. However, for stationary or retreating tips displaying lateral displacement variations of the type shown in Fig. 1b and c this alternative method leads to the erroneous conclusion that propagation has occurred.

For most of the faults examined here the main phase of propagation occurs early during fault growth. A similar observation has been made by Morley (1999) who concluded that "boundary fault propagation to near-maximum length occurs rapidly during the very early stages of rifting". During the later stages of fault growth, fault propagation is reduced. These observations are consistent with a model of fault system evolution where a large population of faults is developed at the early stages of basin extension by the initiation of new faults and by fault propagation (Walsh and Watterson, 1987; Cowie et al., 1993, 1995; Meyer et al., 2002; Walsh et al., 2001). This phase of growth is followed by a period in which fault density approaches saturation and fault propagation is retarded by fault interaction (Morewood and Roberts, 1999). During these later stages, increase in fault length is predominantly by the amalgamation of existing, coeval faults by fault capture and relay zone failure which will ultimately lead to a localisation of strain onto a diminishing number of large active faults (Cowie, 1998; Walsh et al., 2001, 2002).

6. Conclusions

1. Synsedimentary faults for which the rate of sedimentation equals or exceeds the rate of displacement can be analysed to determine their size and throw distribution at the time of deposition of interpreted syn-fault horizons.
2. Throw contours and tip-lines on strike-projections of synsedimentary faults typically show an abrupt change from sub-horizontal within the syn-fault sequence to sub-vertical within the uppermost pre-fault sequence.
3. The dip-parallel spacing of contours within the syn-fault sequence is determined by the relative rates of throw and of sedimentation.
4. Sub-horizontal throw contours are an indicator of synsedimentary fault movement, even where growth indices are low.
5. For propagating synsedimentary faults, tip-lines at earlier stages of growth can be approximately located from the form and positions of throw contours on strike-projections and from fault displacement profiles.
6. Lateral tip-line propagation may cease, or the active tip-line may even retreat, where the strain field of a fault interacts with that of another fault or where fault linkage occurs. In such cases the map traces of syn-fault horizons may be the same length, or shorter, than those of pre-fault horizons.
7. Stasis or retreat of lateral tip-lines result in relatively steep lateral throw gradients, and closely spaced throw contours, in the tip regions of both growth and blind faults.
8. The highest measured tip-line propagation rate for a tectonic normal fault in the areas studied is 3 km/My averaged over a 1.3 My period.
9. Rates of fault propagation decrease with elapsed time from the initiation of faulting, with tip-line stasis and retreat becoming dominant in the later stages of fault growth.

Acknowledgments

We thank staff of BHP Petroleum, Exxon and former

Britoil staff for provision of data. Members of the Fault Analysis Group are thanked for useful discussion. Susannah Anderson Carr helped with preparation of the manuscript. Ben Brooks and Mark Anders are thanked for their helpful reviews. This research was partly funded by EC Hydrocarbon JOULE (contract JOUF-0036-C).

References

Barnett, J.A.M., Mortimer, J., Rippon, J., Walsh, J.J., Watterson, J., 1987. Displacement geometry in the volume containing a single normal fault. Bulletin of the American Association of Petroleum Geologists 71, 925–937.

Benedetti, L., Tapponier, P., King, G.C.P., Meyer, B., Manighetti, I., 2000. Growth folding and active thrusting in the Montello region, Veneto, northern Italy. Journal of Geophysical Research 105, 739–766.

Childs, C., Easton, S.J., Vendeville, B.C., Jackson, M.P.A., Lin, S.T., Walsh, J.J., Watterson, J., 1993. Kinematic analysis of faults in a physical model of growth faulting above a viscous salt analogue. Tectonophysics 228, 313–329.

Childs, C., Watterson, J., Walsh, J.J., 1995. Fault overlap zones within developing normal fault systems. Journal of the Geological Society 152, 535–549.

Contreras, J., Anders, M.H., Scholz, C.H., 2000. Growth of a normal fault system: observations from the Lake Malawi basin of the east African rift. Journal of Structural Geology 22, 159–168.

Cowie, P.A., 1998. A healing–reloading feedback control on the growth rate of seismogenic faults. Journal of Structural Geology 20, 1075–1087.

Cowie, P.A., Sornette, D.C.V., 1995. Multifractal scaling properties of a growing fault population. Geophysical Journal International 122, 457–469.

Cowie, P.A., Vanneste, C., Sornette, D., 1993. Statistical physics model for the spatiotemporal evolution of faults. Journal of Geophysical Research 98, 21809–21821.

Dawers, N.H., Underhill, J.R., 2000. The role of fault interaction and linkage in controlling synrift stratigraphic sequences: Late Jurassic, Statfjord East area, northern North Sea. Bulletin of the American Association of Petroleum Geologists 84, 45–64.

Gawthorpe, R.L., Fraser, A.J., Collier, R.E.L., 1994. Sequence stratigraphy in active extensional basins: implications for the interpretation of ancient basin fills. Marine and Petroleum Geology 11, 642–658.

Gibson, J.R., Walsh, J.J., Watterson, J., 1989. Modelling of bed contours and cross-sections adjacent to planar normal faults. Journal of Structural Geology 11, 317–328.

Gradstein, F.M., Agterberg, F.P., Ogg, J.G., Hardenbol, J., Van Veen, P., Thierry, J., Zehui Huang, 1995. A Triassic, Jurassic and Cretaceous time scale. In: Berggren, W.A., Kent, D.V., Aubury, M.-P., Hardenbol, J. (Eds.), Geochronology, Time Scales and Global Stratigraphic Correlation. Society for Sedimentary Geology Special Publication 54, pp. 95–126.

Huggins, P., Watterson, J., Walsh, J.J., Childs, C., 1995. Relay zone geometry and displacement transfer between normal faults recorded in coal-mine plans. Journal of Structural Geology 17, 1741–1755.

Jackson, J., McKenzie, D., 1983. The geometrical evolution of normal fault systems. Journal of Structural Geology 5, 471–482.

Jackson, J., Leeder, M., 1994. Drainage systems and the evolution of normal faults: an example from Pleasant Valley, Nevada. Journal of Structural Geology 16, 1041–1059.

Jackson, J., Norris, R., Youngson, J., 1996. The structural evolution of active fault and fold systems in central Otago, New Zealand: evidence revealed by drainage patterns. Journal of Structural Geology 18, 217–234.

Larsen, P.-H., 1988. Relay structures in a Lower Permian basement-involved extension system, East Greenland. Journal of Structural Geology 10, 3–8.

Medwedeff, D.A., 1992. Geometry and kinematics of an active, laterally propagating wedge thrust, Wheeler Ridge, California. In: Mitra, S., Fisher, G.W. (Eds.), Structural Geology of Fold and Thrust Belts, Johns Hopkins University Press, Baltimore, pp. 3–27.

Meyer, V., Nicol, A., Childs, C.C., Walsh, J.J., Watterson, J., 2002. Progressive localisation of strain during the evolution of a normal fault population. Journal of Structural Geology 24, 1215–1231.

Morewood, N.C., Roberts, G.P., 1999. Lateral propagation of the surface trace of the South Alkyonides normal fault segment, central Greece: its impact on models of fault growth and displacement–length relationships. Journal of Structural Geology 21, 635–652.

Morley, C.K., 1999. Patterns of displacement along large normal faults: implications for basin evolution and fault propagation, based on examples from East Africa. Bulletin of the American Association of Petroleum Geologists 83, 613–634.

Nicol, A., Watterson, J., Walsh, J.J., Childs, C., 1996. The shapes, major axis orientations and displacement patterns of fault surfaces. Journal of Structural Geology 18, 235–248.

Nicol, A., Walsh, J.J., Watterson, J., Underhill, J.R., 1997. Displacement rates of normal faults. Nature 390, 157–159.

Peacock, D., 1990. Displacements, segment linkage and relay ramps in normal fault zones. PhD thesis, University of Southampton.

Peacock, D.C.P., Sanderson, D.J., 1994. Geometry and development of relay ramps in normal fault systems. The American Association of Petroleum Geologists Bulletin 78, 147–165.

Petersen, K., Clausen, O.R., Korstgård, J.A., 1992. Evolution of a salt-related listric growth fault near the D-1 well, block 5605, Danish North Sea: displacement history and salt kinematics. Journal of Structural Geology 14, 565–577.

Ranalli, G., 1977. Correlation between length and offset in strike-slip faults. Tectonophysics 37, T1–T7.

Rowan, M.G., Hart, B.S., Nelson, S., Flemings, P.B., Trudgill, B.D., 1998. Three dimensional geometry and evolution of a salt related growth fault array: Eugene Island 330 field, offshore Louisiana, Gulf of Mexico. Marine and Petroleum Geology 15, 309–328.

Savage, J.C., 1966. Radiation from a realistic model of faulting. Bulletin of the Seismological Society of America 56, 577–592.

Schlische, R.W., 1991. Half-graben basin filling models: new constraints on continental extensional basin development. Basin Research 3, 123–141.

Walsh, J.J., Watterson, J., 1987. Growth of the dimensions, displacements and displacement profiles of single faults. Geophysical Journal of the Royal Astronomical Society 89, 488.

Walsh, J.J., Watterson, J., 1989. Displacement gradients on fault surfaces. Journal of Structural Geology 11, 307–316.

Walsh, J.J., Watterson, J., 1990. New methods of fault projection for coalmine planning. Proceedings of the Yorkshire Geological Society 48, 209–219.

Walsh, J.J., Childs, C., Meyer, V., Manzocchi, T., Imber, J., Nicol, A., Tuckwell, G., Bailey, W.R., Bonson, C.G., Watterson, J., Nell, P.A.R., Strand, J., 2001. Geometrical controls on the evolution of normal fault systems. In: Holdsworth, R.E. (Ed.), The Nature of the Tectonic Significance of Fault Zone Weakening. Special Publication of the Geological Society of London 186, 157–170.

Walsh, J.J., Childs, C., Imber, J., Manzocchi, T., Watterson, J., Nell, P.A.R., 2002. Strain localisation and population changes during fault system growth. Journal of Structural Geology, in press.

Watterson, J., 1986. Fault dimensions, displacements and growth. Pure and Applied Geophysics 124, 365–373.

Wibberley, C.A.J., Petit, J.P., Rives, T., 1999. Mechanics of high displacement gradient faulting prior to lithification. Journal of Structural Geology 21, 251–257.

Woods, E.P., 1992. Vulcan Sub-basin fault styles—implications for hydrocarbon migration and entrapment. Australian Petroleum Exploration Association Journal 32, 138–158.